

Interaction potential for silicon carbide: A molecular dynamics study of elastic constants and vibrational density of states for crystalline and amorphous silicon carbide

Priya Vashishta,^{a)} Rajiv K. Kalia, and Aiichiro Nakano

Collaboratory for Advanced Computing and Simulations, Department of Chemical Engineering and Materials Science, Department of Physics & Astronomy, and Department of Computer Science, University of Southern California, Los Angeles, California 90089-0242

José Pedro Rino

Departamento de Física, Universidade Federal de São Carlos, São Carlos, SP 13565-905, Brazil and Collaboratory for Advanced Computing and Simulations, Department of Chemical Engineering and Materials Science, Department of Physics & Astronomy, and Department of Computer Science, University of Southern California, Los Angeles, California 90089-0242

(Received 10 October 2006; accepted 6 March 2007; published online 22 May 2007)

An effective interatomic interaction potential for SiC is proposed. The potential consists of two-body and three-body covalent interactions. The two-body potential includes steric repulsions due to atomic sizes, Coulomb interactions resulting from charge transfer between atoms, charge-induced dipole-interactions due to the electronic polarizability of ions, and induced dipole-dipole (van der Waals) interactions. The covalent characters of the Si–C–Si and C–Si–C bonds are described by the three-body potential. The proposed three-body interaction potential is a modification of the Stillinger-Weber form proposed to describe Si. Using the molecular dynamics method, the interaction potential is used to study structural, elastic, and dynamical properties of crystalline (3C), amorphous, and liquid states of SiC for several densities and temperatures. The structural energy for cubic (3C) structure has the lowest energy, followed by the wurtzite (2H) and rock-salt (RS) structures. The pressure for the structural transformation from 3C-to-RS from the common tangent is found to be 90 GPa. For 3C-SiC, our computed elastic constants (C_{11} , C_{12} , and C_{44}), melting temperature, vibrational density-of-states, and specific heat agree well with the experiments. Predictions are made for the elastic constant as a function of density for the crystalline and amorphous phase. Structural correlations, such as pair distribution function and neutron and x-ray static structure factors are calculated for the amorphous and liquid state. © 2007 American Institute of Physics. [DOI: 10.1063/1.2724570]

I. INTRODUCTION

Silicon carbide (SiC) has been proposed for a wide range of technological applications, such as optoelectronic devices and engineering materials, because it has highly useful properties, i.e., excellent chemical stability, good electronic properties, high stiffness, and high hardness. Light weight, high strength, chemical stability, high thermal conductivity, and low thermal expansion of SiC allow for its use in technological applications such as gas turbines, heat exchangers, and ceramic fans. Its wide band gap, high electron mobility, and high barrier for electron breakdown make it ideal for radar, microwave, solar cell, and high-voltage devices.^{1–6} Silicon carbide in the amorphous alloy form, $a\text{-Si}_x\text{C}_{1-x}$, is of additional technological interest due to the temperature stability of its tuning semiconducting properties, which allows unique applications under extreme conditions such as high-temperature engines, turbines, and reactors.²

At ambient pressure, there exists various polytypes in SiC originating from differences in the stacking sequence of the silicon-carbon pair layer.^{3,7} Besides the cubic β -SiC, SiC has a unique property that it shows polytypism⁸ with about

70 hexagonal and 170 rhombohedral structures. In all these polytypes, the chemical bonds characterized by covalent sp^3 bonding are identical and the tetrahedrally coordinated properties are almost the same.⁹ Among the polytypes, the zinc-blende structure is the most common.

It is important to study the phase stability of materials under high pressures for microscopic understanding as well as technological applications.¹⁰ For this purpose inelastic neutron scattering and neutron diffraction studies have been used with success to describe the structure and dynamics of amorphous and glassy materials.^{11–19} To the best of our knowledge there are no such neutron scattering studies of amorphous silicon carbide ($a\text{-SiC}$), but several other experimental and theoretical studies of $a\text{-SiC}$ were performed.

For the last few decades, there have been a number of experimental^{20–24} and theoretical^{23–28} studies on the structural transformation under high pressure in SiC. Yoshida *et al.*²⁰ have found from x-ray diffraction measurements that SiC transforms from the fourfold coordinated zinc-blende structure to a sixfold coordinated rock salt structure at a pressure above 100 GPa, with a 20.3% volume reduction. In their experiments they have observed a large hysteresis associated with this phase transformation. In the reverse transformation,

^{a)}Electronic mail: priyav@usc.edu

when the pressure is decreased, a transformation from the rock-salt structure to the zinc-blende structure takes place at a pressure below 35 GPa. Shock compression experiments²¹ also suggest that the high-pressure phase of SiC above 100 GPa has rock-salt structure. Theoretical studies^{23,24,29} based on *ab initio* pseudopotential calculations predict the transition pressure to be around 60 GPa, which is in reasonable accord with the experiments.

Numerous other experimental techniques such as x-ray diffraction, extended x-ray absorption fine structure (EXAFS), x-ray photo emission, Raman and infrared spectroscopy, and extended electron-energy-loss (EXELFS) have been performed in order to study high-pressure transformation and chemical bond order, in both crystalline and amorphous SiC, and in hydrogenated *a*-SiC:H materials.³⁰⁻³⁷ However, only a few theoretical interaction potentials have been published for SiC. A simple rigid ion model was used by Vetelino and Mitra³⁸ to calculate the phonon-dispersion curves; Chang and Cohen,²³ Park *et al.*,³⁹ and Karch²⁸ used *ab initio* electronic structure method with pseudopotentials to study structural properties of SiC at low and high pressures, while Finocchi *et al.*⁴⁰ performed *ab initio* molecular dynamics simulation on equimolar Si-C amorphous alloy, and Ivashchenko *et al.*⁴¹ studied amorphous SiC through molecular dynamics in the framework of an sp^3s^* tight-binding force model. A bond charge model was used by Zywiets *et al.*⁴² to study the influence of polytypism on thermal properties of SiC, and the full-potential linear-muffin-tin combined with local density function theory was used by Lambrecht *et al.*⁴³ to study elastic constants and deformation potentials in cubic SiC. Kelires⁴⁴ has used the interaction potential proposed by Tersoff⁴⁵ to perform Monte Carlo simulations, and Tang *et al.*,⁴⁶ Porter *et al.*,⁴⁷ Li *et al.*,⁴⁸ and Noreyian *et al.*⁴⁹ have used molecular dynamics methods to study elastic and thermal properties of SiC. Brittle fracture of cubic SiC under hydrostatic pressure was simulated using Tersoff potential by Tang and Yip.⁵⁰ Surface reconstruction and thermal stability in cubic SiC has been described both by *ab initio*⁵¹ and classical⁵² (Tersoff potential) molecular dynamics simulations. Simulation of sublimation growth⁵³ and defect generation in irradiated and amorphization on 3C-SiC⁵⁴⁻⁵⁷ has also been reported. Huang *et al.*⁵⁸ compared the defect energetic through Tersoff,⁴⁵ Pearson,⁵⁹ and modified embedded-atom (MEAM) potentials. Recently, Erhart and Albe⁶⁰ have proposed an analytical bond-order form⁶¹ to describe elastic, thermal, and point defect in Si, C, and SiC. Empirical bond-order potentials by Tersoff⁴⁵ and others^{60,62} have been used successfully to describe elastic and thermal properties of SiC. What has been less studied with these potentials is the high-pressure structural transformation of SiC, in particular its atomistic mechanisms. The interatomic potential proposed in this paper has been used to predict a new transformation pathway,⁶³ which was later confirmed by first-principles quantum-mechanical calculations in the framework of the density functional theory (DFT).^{64,65} Another essential mechanical property less studied with the bond-order potentials is the fracture toughness for various crystallographic orientations, for which our interatomic potential provides good agreement with available experimental values.⁶⁶ As we

present in this paper, unstable stacking fault energies calculated with our interatomic potential also agree well with first-principles DFT values, which are critical for the study of plasticity in SiC.

In this paper, we report an interatomic interaction potential for SiC. We study the elastic properties of cubic and amorphous SiC phases, its vibrational density of states, and the structure of the molten phase by total and partial pair distribution functions, structure factors, and coordination numbers. The paper is divided into eight sections. In Sec. II we describe the interaction potential and give the parameters for the two- and three-body parts of the potential; in Sec. III we discuss the structural energies and melting of SiC; in Sec. IV we present and discuss the results for elastic properties of crystalline and amorphous SiC. In Sec. V the structural transformation induced by pressure as well as surface and stacking fault energies are analyzed. Section VI discusses the vibrational density of states for 3C-SiC and *a*-SiC, Sec. VII is devoted to molten properties, and finally we present the conclusions in Sec. VIII.

II. INTERACTION POTENTIAL FOR SiC

Complex chemical bonds in SiC involve both ionic and covalent characters. There is charge transfer between Si and C atoms resulting in Coulomb interaction between ions, so the two-body interaction potential must contain at a minimum a steric repulsion as well as Coulomb interactions. However, such a simple two-body interaction is not sufficient to describe the effect of other interactions present in a material like SiC. In addition, a three-body potential is needed to describe the covalent character of bond bending and stretching.

Our effective interatomic interaction potential consists of two- and three-body interactions. The total potential energy of the system is given by

$$V = \sum_{i < j} V_{ij}^{(2)}(r_{ij}) + \sum_{i, j < k} V_{jik}^{(3)}(r_{ij}, r_{ik}). \quad (1)$$

Based on the form of our earlier interaction potential for AgI,⁶⁷⁻⁶⁹ the two-body interaction potential includes steric size effects of the ions, charge-transfer effects leading to Coulomb interactions, charge-dipole interactions due to the electronic polarizability of ions, and induced dipole-dipole (van der Waals) interactions. The two-body part of the effective potential is written as

$$V_{ij}^{(2)}(r) = \frac{H_{ij}}{r^{\eta_{ij}}} + \frac{Z_i Z_j}{r} e^{-r/\lambda} - \frac{D_{ij}}{2r^4} e^{-r/\xi} - \frac{W_{ij}}{r^6}. \quad (2)$$

Here, H_{ij} is the strength of the steric repulsion, Z_i the effective charge (in units of the electronic charge $|e|$), D_{ij} the strength of the charge-dipole attraction, W_{ij} is the van der Waals interaction strength, η_{ij} the exponents of the steric repulsion term, $r \equiv r_{ij} = |\mathbf{r}_i - \mathbf{r}_j|$ the distance between the i th atom at position \mathbf{r}_i and the j th atom at position \mathbf{r}_j , and λ and ξ are the screening lengths for Coulomb and charge-dipole terms, respectively.

In order to properly account for the short-range order in a tetrahedrally coordinated covalent material, Stillinger and

TABLE I. Parameters for two- and three-body parts of the interaction potential used in the MD simulation of structural, dynamical, and mechanical properties of SiC.

	Si		C			
	$Z_i(e)$	1.201	-1.201			
Two-body		Si-Si	Si-C	C-C		
	η_{ij}	7	9	7		
	H_{ij} (eV Å ^{η})	23.67291	447.09026	471.74538		
	D_{ij} (e ² Å ³)	2.1636	1.0818	0		
	W_{ij} (eV Å ⁶)	0	61.4694	0		
	$\lambda=5.0$ Å	$\xi=3.0$ Å	$r_c=7.35$ Å	e =electronic charge		
		B_{ijk} (eV)	$\bar{\theta}_{ijk}$ (°)	C_{ijk}	γ (Å)	r_0 (Å)
Three-body	Si-C-Si	9.003	109.47	5.0	1.0	2.90
	C-Si-C	9.003	109.47	5.0	1.0	2.90

Weber⁷⁰ introduced an r -dependent function in the three-body angle-dependent form which has been proposed by Keating.⁷¹ We propose a three-body effective interaction potential which is an important modification of the Stillinger-Weber⁷⁰ form. Our new three-body form is necessary to describe the structural transformation under pressure and melting behavior of the material while maintaining the bond-bending and bond-stretching characteristics. It is written as a product of the spatial and angular dependence as

$$V_{jik}^{(3)}(r_{ij}, r_{ik}) = R^{(3)}(r_{ij}, r_{ik}) P^{(3)}(\theta_{jik}), \quad (3)$$

where

$$R^{(3)}(r_{ij}, r_{ik}) = B_{jik} \exp\left(\frac{\gamma}{r_{ij} - r_0} + \frac{\gamma}{r_{ik} - r_0}\right) \Theta(r_0 - r_{ij}) \Theta(r_0 - r_{ik}), \quad (4)$$

$$V_{ij}^{(2 \text{ shifted})}(r) = \begin{cases} V_{ij}^{(2)}(r) - V_{ij}^{(2)}(r_c) - (r - r_c)(dV_{ij}^{(2)}(r)/dr)_{r=r_c} & r \leq r_c \\ 0 & r > r_c \end{cases}. \quad (6)$$

The parameters in the interaction potential were determined using a few selected physical properties such as cohesive energy, bulk modulus, and C_{11} elastic constant at the experimental density of 3C-SiC. Table I summarizes the parameters for SiC interaction potential.

In Fig. 1 we show the shifted $V^{(2)}$ interaction potential as a function of distance, and the angular three-body interaction potential $P^{(3)}$ is shown in Fig. 2. Note that while in the Keating and Stillinger-Weber potential the angular dependence increases indefinitely when the angle deviates from the equilibrium angle, our proposed modification has the same dependence around the equilibrium angle, but saturates for a large deviation from the equilibrium angle. This allows for the reconfiguration of bonds in structural transformation under pressure and in melting. In Table II we summarize quantities calculated using our interaction potential and the corresponding experimental values.

$$P^{(3)}(\theta_{jik}) = \frac{(\cos \theta_{jik} - \cos \bar{\theta}_{jik})^2}{1 + C_{jik}(\cos \theta_{jik} - \cos \bar{\theta}_{jik})^2}. \quad (5)$$

In this three-body interaction potential, B_{jik} is the strength of the interaction, θ_{jik} the angle formed by \mathbf{r}_{ij} and \mathbf{r}_{ik} , and C_{jik} and $\bar{\theta}_{jik}$ are constants. $\Theta(r_0 - r_{ij})$ is the step function.

Based on previous experience^{68,72-74} the exponents η_{ij} were chosen to be 7, 9, and 7, respectively, for Si-Si, Si-C, and C-C interactions. The screening lengths were fixed to be $\lambda=5.0$ Å and $\xi=3.0$ Å. For computational efficiency, the two-body interaction is truncated at $r=r_c$ (7.35 Å), and shifted for $r < r_c$ in order to have the potential and its first derivative continuous at r_c .^{75,76} The three-body part is short ranged due to the r -dependence of Eq. (4). The expression for the shifted two-body part of the potential is

III. STRUCTURAL ENERGIES AND MELTING

The lattice energy, for different crystalline structures, is calculated as a function of volume. These calculations allow

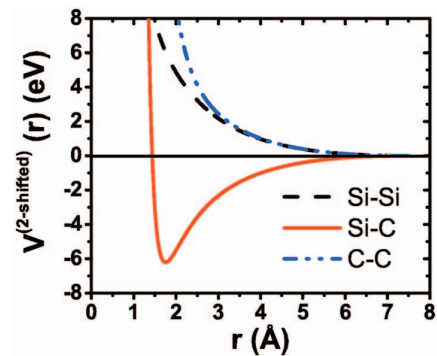


FIG. 1. (Color) Two-body interaction potential as a function of distance, as described in Eq. (6).

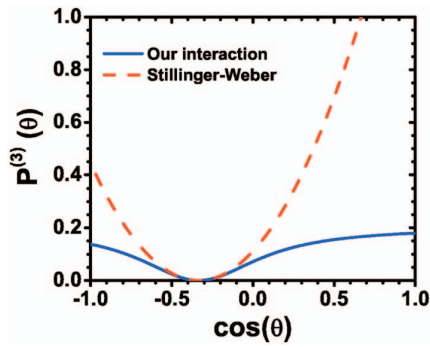


FIG. 2. (Color) Angular dependence of our three-body interaction potential defined in Eq. (3), continuous curve. For comparison the Stillinger-Weber three-body interaction potential is also displayed, dashed curve. In this plot the constant angle $\theta=109.47^\circ$ and $C=5$, as given in Table I.

us to predict the most stable structures, their equilibrium energy, lattice constant, bulk modulus and its derivative, and the pressure necessary to induce a structural transformation. All MD calculations reported in this paper consists of a system with 4096 atoms (2048 Si+2048 C) initially in a cubic zinc-blende structure. The cubic cell edge L has 34.8648 Å, which reproduces the experimental density of 3.2175 g/cc.

A. Structural energies for zinc-blende, wurtzite, and rock-salt structures

The energetic for zinc-blended (ZB), wurtzite (2H), and rock-salt (RS) structures is calculated as a function of volume per atom. The lattice parameters for 2H structure is taken from Park *et al.*³⁹ In Fig. 3 all three energies are shown plotted as a function of volume for zinc blende, wurtzite (2H), and rock-salt structures. The energies were obtained by hydrostatic compression/dilation of the unit cells.

For each curve a Murnaghan equation of state⁷⁷

$$E(V) = \frac{BV}{B'(B'-1)} \left[B' \left(1 - \frac{V_0}{V} \right) + \left(\frac{V_0}{V} \right)^{B'} - 1 \right] + E(V_0) \quad (7)$$

was fitted (shown as dashed lines in Fig. 3), and the results are summarized in Table III together with the values obtained from MD at zero pressure. From a common tangent between

TABLE II. Calculated and experimental values for a selected number of physical quantities for 3C-SiC.

	Experiments	MD
Lattice constant (Å)	4.3596 ^a	4.3581
Cohesive energy (eV)	6.34 ^b	6.3410868
Melting/decomposition temperature (K)	3103±40 ^b	3250±50
Bulk modulus (GPa)	225–270 ^{b,d}	225.2
Elastic constants (GPa)		
C_{11}	390 ^d	390.0
C_{12}	142 ^d	142.6
C_{44}	150–256 ^{b,d}	191.0

^aReference 92.

^bReference 91.

^cReference 93.

^dReference 94.

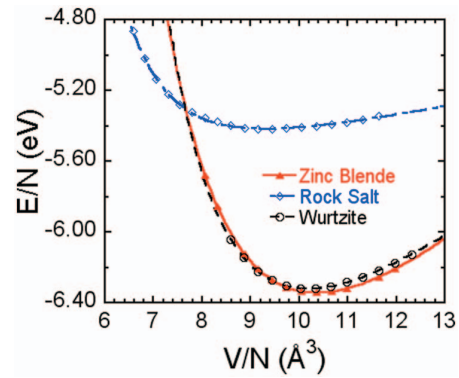


FIG. 3. (Color) Energy per particle as a function of volume per particle. The difference in energy per particle between zinc-blende and wurtzite structures is $\Delta E=0.022$ eV. Dashed lines are a fit of Murnaghan equation of state, Eq. (7). A common tangent between zinc-blende and rock-salt energy curves determines the pressure of the structural transformation to be around 90 GPa. Energy at the 3C-SiC minima is -6.342 eV at the unit cell volume $V_0=82.744 \text{ \AA}^3$ ($a_0=4.3574 \text{ \AA}$) and the corresponding minima for wurtzite is -6.320 eV at the unit cell volume $V_0=81.52 \text{ \AA}^3$ ($a_0=3.061 \text{ \AA}$, $c=5.023 \text{ \AA}$).

the ZB and RS structures, it is possible to infer that the pressure of structural transformation to be around 90 GPa. From the Murnaghan equation of state, it was found that 3C-SiC crystal structure has its minimum energy at -6.342 eV and the unit cell volume is $V_0=82.744 \text{ \AA}^3$, which corresponds to a unit cell lattice constant of $a_0=4.3574 \text{ \AA}$. Wurtzite, on the other hand, has the minimum energy of -6.320 eV at the unit cell volume of $V_0=81.52 \text{ \AA}^3$, which corresponds to a lattice constant of $a=3.061 \text{ \AA}$, $c=5.023 \text{ \AA}$, whose ratio is $c/a=1.6409$, in very good agreement with the experiment,⁸ which gives $c/a=1.641$. The difference in energy per particle between these two structures is only $\Delta E=0.022$ eV, ZB being more stable than the 2H structure.

TABLE III. Molecular dynamics results, Murnaghan equation of state fit to the MD data, and experimental data for minimum energy per particle, volume of the unit cell, bulk modulus, B , and first derivative of the bulk modulus, B' , for zinc-blende, wurtzite, and rock-salt structures. For rock salt the cohesive energy and bulk modulus are calculated at the minimum of the energy vs volume curve shown in Fig. 3.

		Molecular dynamics	Murnaghan equation of state	Experimental results
Zinc blende	E/N (eV)	-6.34109	-6.342	-6.34 ^a
	V/N (\AA^3)	10.3467	10.36	10.3574 ^c
	B (GPa)	225.2	231.3	224–269
	B'	-	5.5	4.1 ^b
Wurtzite	E/N (eV)	-6.31953	-6.320	
	V/N (\AA^3)	10.3410	10.184	10.3410 ^d
	B (GPa)	228.9	221.5	223–225 ^{c,d}
	B'	-	6.9	
Rock salt	E/N (eV)	-5.41987	-5.419	
	V/N (\AA^3)	9.3273	9.4479	
	B (GPa)	96.1	71.2	
	B'	-	5.2	

^aReference 91.

^bReference 95.

^cReference 93.

^dReference 39.

^eReference 97.

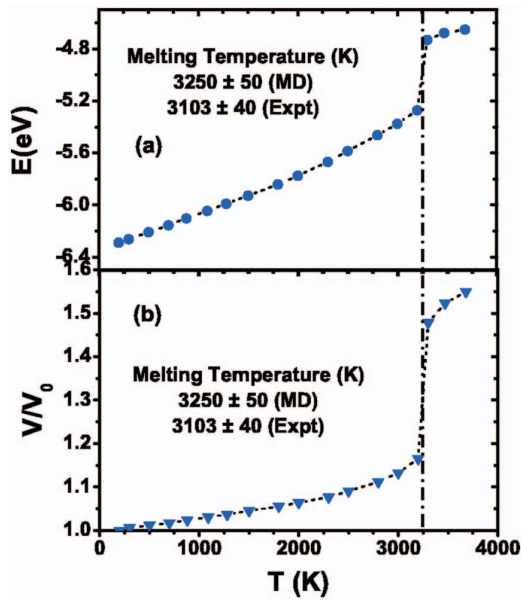


FIG. 4. (Color) Energy per particle and volume ratio, V/V_0 , as a function of temperature. V_0 is the volume of the system at zero temperature. Dotted lines are a guide for the eye and the vertical dashed dotted line represents the calculated melting temperature of 3250 K.

B. Melting of 3C-SiC

The molten state was prepared by continuously heating the 3C-SiC crystalline structure, using the constant-pressure, constant-temperature MD method. Starting from its ZB structure at 300 K, the system was heated in steps of 200 K at constant pressure. At each temperature, the system was thermalized for 40 000 time steps (one time step $\Delta t=2.0$ fs) before further heating. In Fig. 4(a) the energy per particle is displayed and in Fig. 4(b) the volume ratio as a function of temperature. The dotted line at $T=3250\pm 50$ K indicates the calculated melting temperature of the 3C-SiC crystal, which agrees quite well with the reported experimental melting temperature of 3103 ± 40 K measured at 35 bars.⁷⁸

It should be pointed out here that the molecular dynamics melting temperature should be higher than the experimental one, because in the simulation we are dealing with a perfect crystal and the effects due to the periodic boundary conditions are present. The MD melting temperature tends to decrease as the system size increases. In addition, the presence of defects also lowers the melting temperature. Therefore, for a perfect crystal of 4096 atoms with periodic boundary conditions, the agreement between the MD melting temperature, 3250 ± 50 K, and the experimental value, 3103 ± 40 K, (an infinite system with defects) is indeed excellent.

IV. ELASTIC PROPERTIES OF CRYSTALLINE AND AMORPHOUS SiC

Elastic constants of a materials can be measured, in principle, through several different techniques such as ultrasonic wave propagation, Brillouin scattering, neutron scattering, among others. We have computed the elastic properties of SiC to compare with the available experimental data. Predictions

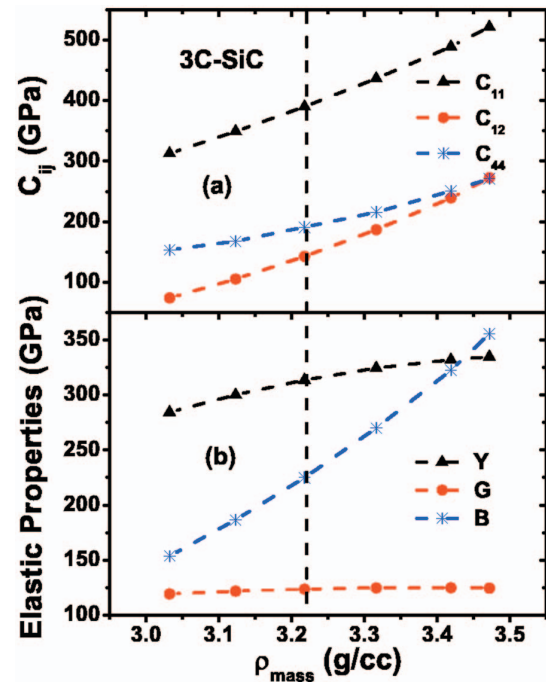


FIG. 5. (Color) Calculated elastic properties for 3C-SiC as a function of density. (a) Elastic constants C_{11} , C_{12} , and C_{44} ; (b) Young modulus, Y , shear modulus, G , and bulk modulus, B . The vertical dashed line corresponds to the experimental density of $\rho=3.217$ g/cm³.

tions of elastic constants are also made for crystalline and amorphous SiC. With the proposed interaction potential, the linear elastic constants were calculated at zero temperature directly from the stress-strain relationship, i.e., $C_{\alpha,\beta,\mu,\nu} = \partial\sigma_{\alpha,\beta} / \partial\varepsilon_{\mu,\nu}$ where σ is the external applied stress and ε the strain.⁷⁹

A. Elastic properties of 3C-SiC

Figure 5(a) summarizes the results of the elastic constants calculated for 3C-SiC as a function of density. The most common elastic moduli are the Young modulus, the Poisson ratio, bulk modulus, and the shear modulus, which are displayed in Fig. 5(b) (dashed lines are only to guide the eye). The vertical dashed line marks the observed crystalline density. Young modulus was determined through $Y=(C_{11}+2C_{12})(C_{11}-C_{12})/(C_{11}+C_{12})$, Poisson ratio through $\nu=C_{12}/(C_{11}+C_{12})$, shear modulus by $G=Y/[2(1+\nu)]$, and bulk modulus by $B=Y/[3(1-2\nu)]$. Bulk modulus has a strong dependence with the density of the material, Young modulus a weak dependence, while the shear modulus is practically independent of density.

B. Elastic properties of amorphous SiC

For amorphous SiC the elastic constants have similar dependence on density as that observed in the cubic crystal structure, Fig. 6(a). However, as displayed in Fig. 6(b), the Y , B , and G moduli show significantly different behavior. All three elastic moduli for amorphous SiC show more pronounced nonlinearity with density when compared to the crystalline case.

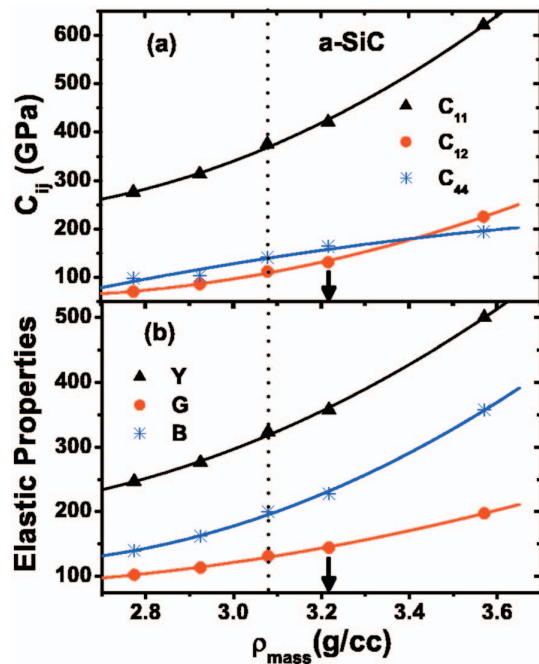


FIG. 6. (Color) Elastic properties for amorphous SiC. (a) Calculated elastic constants and shear, $C_{44}=(C_{11}-C_{12})/2$, as a function of density; (b) Young modulus, Y , shear modulus, G , and bulk modulus, B . The solid arrow marks the observed 3C-SiC density (3.217 g/cc) and the vertical dashed line marks the density (3.076 g/cc) at which the amorphous SiC has zero internal pressure.

Finally, in Table IV the mechanical properties calculated for 3C-SiC and amorphous SiC are compared with the available experimental data. It is worth mentioning that the agreement with the experimental data for 3C-SiC is not fortuitous, since only C_{11} and B were used as input data in the parametrization of the interaction potential. Furthermore, we are making predictions for the elastic properties for the amorphous phase.

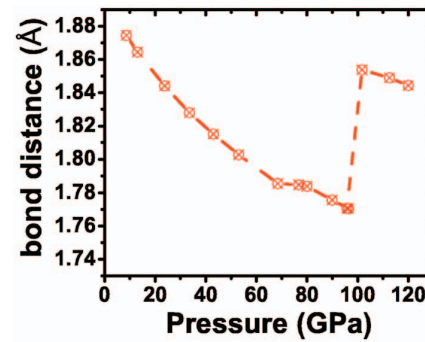


FIG. 7. (Color) Si-C bond distance as a function of applied pressure.

V. ZINC-BLENDE TO ROCK-SALT STRUCTURAL TRANSFORMATION UNDER PRESSURE, SURFACE ENERGY, AND STACKING FAULT ENERGY FOR SiC

A. Structural transformation under pressure

The energy versus atomic volume, Fig. 3, correctly predicts the pressure of transformation between zinc-blende and rock-salt structures. This structural transformation could be observed dynamically from our MD simulations. Starting at zero pressure the system was first heated up to 1800 K. At this fixed temperature the external pressure was increased in steps of 5 GPa up to 140 GPa. For each applied pressure the system is allowed to run for 20 000 time steps. The averages of the physical quantities were taken over additional 10 000 time steps. Figure 7 shows the Si-C bond distance defined as the peak position of the partial Si-C pair correlation function, as a function of the applied pressure. Up to 80 GPa the system responds with elastic compression. Around 110 GPa the bond length suddenly increases, and with further increase of pressure the elastic compression is again observed in the new structure. Pair distribution function and bond angles for two pressures, above and below the transformation, depicted in Figs. 8(a) and 8(b), confirm the transformation. The four-fold coordinated system, which has a characteristic Si-C-Si bond angle peaked at 109° , changes to sixfold coordination number with Si-C-Si bond angle peaked at 90° and 180°

TABLE IV. Elastic constants, bulk modulus, B , Young modulus, Y , shear modulus G , as well as Poisson ratio ν , are calculated using our proposed interaction potential, together with the experimentally reported values. Predictions are made for the elastic properties of the amorphous phase, a -SiC.

		C_{11} (GPa)	C_{12} (GPa)	C_{44} (GPa)	B (GPa)	Y (GPa)	G (GPa)	ν
MD results	3C-SiC (3.217 g/cc)	390.1	142.7	191.0	225.1	313.6	123.7	0.268
	a -SiC (at zero pressure, 3.079 g/cc)	375.3	112.5	141.7	200.1	323.4	131.4	0.231
Experiment	3C-SiC	390 ^a	142 ^a	256 ^a	225 ^a	314.2 ^d	124 ^d	0.267 ^d
						694 ^c	192 ^b	0.267 ^a

^aReference 94.

^bReference 93.

^cReference 96.

^dCalculated using the measured values of C_{11} and C_{12} and the definitions $Y=(C_{11}-C_{12})(C_{11}+2C_{12})/(C_{11}+C_{12})$, $\nu=C_{12}/(C_{11}+C_{12})$, $G=Y/[2(1+\nu)]$, $B=Y/[3(1-2\nu)]$.

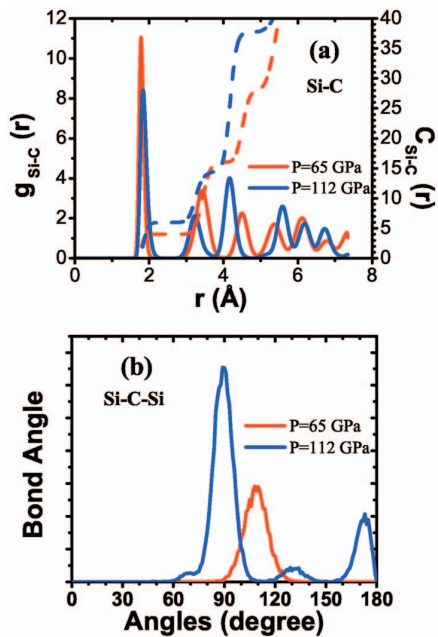


FIG. 8. (Color) (a) Si-C pair distribution function and coordination number as a function of pressure, and the corresponding (b) Si-C-Si bond angle distribution.

characteristic of the rock-salt structure. This structural phase transformation induced by pressure is in excellent agreement with experimental reported data.²⁰

B. Surface energy

The total energy of the system was calculated for bulk, where periodic boundary condition was applied in all directions in order to remove surface dependence, and considering two vacuum regions, above and below, the [110] surface along the c axis. For the former case the system energy was calculated with and without relaxation. The difference between bulk and vacuum setup allows us to obtain the surface energy of the system. For unrelaxed and relaxed surfaces, the surface energy per square angstroms is:

for unrelaxed case:

$$E_{\text{surface}} = 0.1157 \text{ eV}/\text{\AA}^2;$$

for relaxed case:

$$E_{\text{surface}} = 0.1082 \text{ eV}/\text{\AA}^2$$

As far as we know, there is no experimental result available for this quantity.

C. Stacking fault energy

The energy barrier for plastic deformations in SiC is estimated calculating the generalized stacking fault energy for rigid sliding in the {111} plane of the SiC zinc blende by both MD and *ab initio* quantum-mechanical calculations based on the density functional theory (DFT).^{80,81} The electronic-structure calculations are based on the generalized gradient approximation for the exchange-correlation energy.^{80,82,83} The ultrasoft pseudopotential is employed for

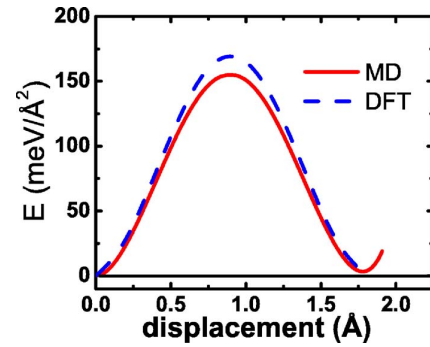


FIG. 9. (Color online) Generalized stacking fault energy for 3C-SiC calculated from MD (continuous line) and DFT (dashed line) (private communication).

the interaction between the valence electrons and ions. The electronic wave functions are expanded by the plane-wave basis set. The energy functional is minimized using an iterative scheme based on the preconditioned conjugate-gradient method^{82,84} with a sufficient k -point sampling in the first Brillouin zone.

The generalized stacking fault energy calculation procedure follows that of Tadmor and Hai⁸⁵ adapted to the zinc-blende crystal. A bulk single-crystal sample with 20 atomic layers in the [111] direction was set up. Vacuum layers were added in the [111] extremes, creating (111) surfaces that were relaxed for 10 000 steps. The relaxation was achieved by quenching the temperature to 0 K by scaling the velocities by a factor of 0.7 every 10 time steps. A set of 10 layers, half the system, was then rigidly slid, against the remaining 10 layers, on the (111) glide plane in the [101] direction using 100 steps forming an intrinsic stacking fault. Each atomic configuration generated during the sliding was relaxed for 10 000 steps in the [111] perpendicular direction, in order to get a minimum energy configuration. The energetics of the rigid sliding shows good agreement between MD and DFT results. The value of the unstable stacking fault energy is $154 \text{ meV}/\text{\AA}^2$ (MD) and $169 \text{ meV}/\text{\AA}^2$ (DFT), the intrinsic stacking fault energy is $5 \text{ meV}/\text{\AA}^2$ (MD) and $1.5 \text{ meV}/\text{\AA}^2$ (DFT) (see Fig. 9). The DFT calculations for the stacking fault energy are from Shimojo (private communications).

VI. VIBRATIONAL DENSITY OF STATES FOR CRYSTALLINE AND AMORPHOUS SiC

The vibrational density of states (VDOS) was obtained from Fourier transformation of the velocity auto-correlation function defined as

$$Z_{\alpha}(t) = \frac{\langle \mathbf{v}_{i\alpha}(0) \cdot \mathbf{v}_{i\alpha}(t) \rangle}{\langle \mathbf{v}_{i\alpha}(0)^2 \rangle}, \quad (8)$$

where $\mathbf{v}_{i\alpha}(t)$ is the velocity of the i th atom of species α (Si or C) at time t and the brackets denote averages over atoms and time origins.

After the system was thermalized at 300 K, the velocity auto-correlation function as a function of time was generated and the vibrational density of states calculated by Fourier transformation of the correspondent partial velocity autocorrelation function,

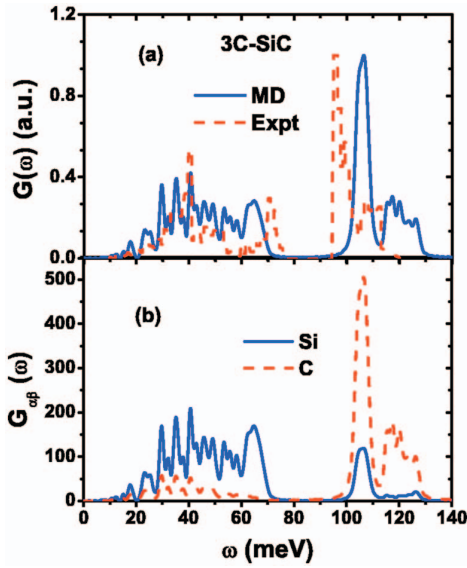


FIG. 10. (Color) (a) Vibrational density of states from MD and experimental density of states obtained from phonon dispersion relations; (b) partial density of states for Si and C from MD.

$$G_{\alpha}(\omega) = \frac{6N_{\alpha}}{\pi} \int_0^{\infty} Z_{\alpha}(t) \cos(\omega t) dt, \quad (9a)$$

and the total vibrational density of states, defined as

$$G(\omega) = \sum_{\alpha} G_{\alpha}(\omega), \quad (9b)$$

was obtained.

A. Vibrational density of states for 3C-SiC

The calculated VDOS is plotted against experimental phonon density of states.⁸⁶ Although the MD optical mode is shifted to higher energies, the gap and the two complex optical modes are correctly described. From the partial VDOS [see Fig. 10(b)] the peak at 64 meV is mainly due to Si vibrations, while most of the modes at high frequency are due to carbon vibrations.

B. Specific heat for 3C-SiC

The specific heat at constant volume can be written as:

$$C_V = \frac{3Nk_B \int_0^{\infty} \frac{u^2 e^u}{(e^u - 1)^2} G(\omega) d\omega}{\int_0^{\infty} G(\omega) d\omega}, \quad (10)$$

where $u = \hbar\omega/k_B T$ and k_B is the Boltzmann constant. With the vibrational density of states discussed above, the specific heat is evaluated from Eq. (10). In Fig. 11(a), $C_V/(3Nk_B)$ is shown as a function of temperature along with the experimental values of C_p at constant pressure. As expected, C_p is larger than calculated C_V at constant volume.

At low temperatures the Debye temperature, Θ_D , can be approximated by $C_V = \frac{12}{5} \pi^4 Nk_B (T/\Theta_D)^3$ and the result is re-

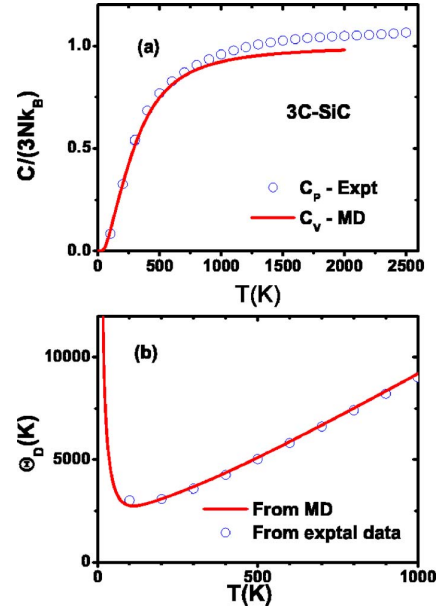


FIG. 11. (Color online) (a) Calculated specific heat at constant volume, C_V and experimental C_p as a function of temperature for 3C-SiC. (b) Debye temperature is calculated using the well-known low-temperature expression $C_V = \frac{12}{5} \pi^4 Nk_B (T/\Theta_D)^3$. Continuous lines are our calculated results and the open circles experimental results calculated using C_p (Ref. 87).

vealed in Fig. 11(b). Using the experimental specific heat data⁸⁷ and the above expression, the “experimental” Debye temperature is also plotted up to 1000 K. The agreement between MD and experimental Θ_D is excellent for all range of temperature up to 1000 K.

C. Vibrational density of states for amorphous SiC

The vibrational density of states was calculated at 300 K for the amorphous system at four different densities. In Fig. 12 the VDOS is shown for a-SiC at crystalline density (3.217 g/cc). Contrary to the density of states in the cubic phase, there is no gap for amorphous SiC. There are just two broad bands with a large contribution of C vibrations at high frequencies and a small contribution at low frequencies. The situation for Si is opposite—large contribution at low frequencies and small contribution at high frequencies.

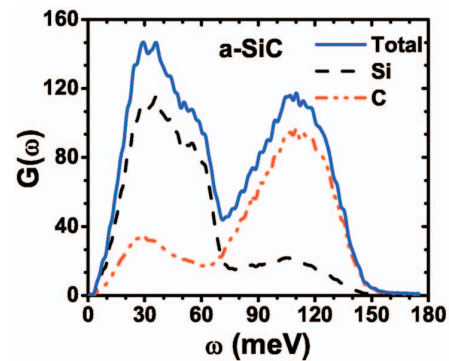


FIG. 12. (Color) MD vibrational density of states and partial densities of states for amorphous SiC at density of 3.217 g/cc.

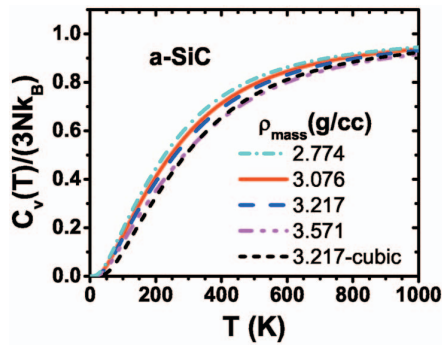


FIG. 13. (Color) Constant volume specific heat C_v calculated from the MD vibrational density of states for amorphous SiC for several densities. Results for 3C-SiC at 3.217 g/cc are also shown.

D. Specific heat for amorphous SiC

From the MD density of states the same procedure was done, as in the crystalline state, to calculate the specific heat at constant volume for the amorphous phase. In Fig. 13 the specific heat as a function of temperature for four densities of amorphous SiC is shown. For comparison, the calculated specific heat for the cubic crystalline phase is also displayed. As we have shown,⁸⁸ the smaller the density, the more nanovoids will be present in the material, and, for a fixed temperature, the specific heat will be higher due to increased number of low-frequency phonons.

The density of 3.076 g/c is the density of a-SiC in which the internal pressure is zero and 3.571 g/cc was the highest density of the simulated amorphous system. Observe that at this density the specific heat resemble that of crystalline 3C-SiC.

VII. MOLTEN SiC

The structural correlations for the molten state were studied at 4000 K.

A. Pair distribution function

The two-body pair distribution, $g(r)$, was calculated from the definition

$$\langle n_{\alpha\beta}(r) \rangle \Delta r = 4\pi r^2 \rho c_\beta \Delta r g_{\alpha\beta}(r), \quad (11)$$

where ρ is the total number density, $n_{\alpha\beta}(r)\Delta r$ is the number of β -particles in a shell between r and $r+\Delta r$ around an α -particle, c_β is the concentration of β -particles, and the brackets denotes ensemble average as well the averages over all α -particle. The coordination number $C_{\alpha\beta}(r)$, which determines the average number of β -particles around an α -particles, is an integral of the corresponding partial pair distribution function

$$C_{\alpha\beta}(R) = 4\pi\rho c_\beta \int_0^R r^2 g_{\alpha\beta}(r) dr. \quad (12)$$

The total pair distribution function, neutron distribution function and charge-charge distribution functions are, respectively, defined as⁷⁴

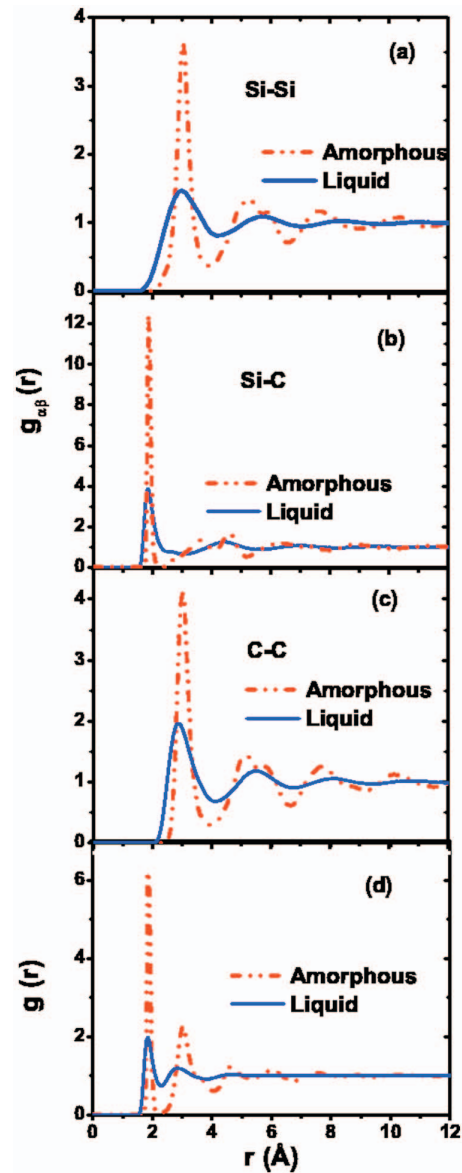


FIG. 14. (Color) Comparison of the pair distribution functions between liquid SiC at 4000 K and amorphous SiC at 300 K. Si-C bond length as well as Si-Si and C-C nearest distance remain practically unchanged in the liquid.

$$g(r) = \sum_{\alpha,\beta} c_\alpha c_\beta g_{\alpha\beta}(r), \quad (13)$$

$$g_n(r) = \frac{\sum_{\alpha,\beta} c_\alpha b_\alpha c_\beta b_\beta g_{\alpha\beta}(r)}{\left(\sum_\alpha c_\alpha b_\alpha \right)^2}, \quad (14)$$

where c_α is the concentration of α -type atoms and b_α is the coherent neutron scattering cross section for α -type atom nuclei.

The structural correlations for the liquid phase are displayed in Fig. 14. Like other tetrahedrally coordinated systems,⁷⁴ the liquid SiC has a very well-defined Si-C bond

length with coordination of 4, up to 2.4 Å as in the amorphous phases. The short range order still is made of well-defined tetrahedra. Although the first peak for all correlations resembles the peaks observed in the amorphous phase with the corresponding thermal broadening, the other coordination shells have their peaks shifted to larger values of r , in the liquid phase, representing larger thermal disorder. There are practically no significant correlations in the molten phase after 5 Å, as shown in Fig. 14(d).

B. X-ray and neutron static structure factors for molten SiC

The Fourier transform of the partial pair distribution function determines the corresponding partial static structure factor, i.e.,

$$S_{\alpha\beta}(q) = \delta_{\alpha\beta} + 4\pi\rho(c_{\alpha}c_{\beta})^{1/2} \int_0^{\infty} [g_{\alpha\beta}(r) - 1] \frac{r^2 \sin(qr)}{qr} dr. \quad (15)$$

From these partial static structure factors we can compute the neutron, x-ray, and charge-charge static structure factors, respectively, as

$$S_n(q) = \frac{\sum_{\alpha,\beta} b_{\alpha}b_{\beta}(c_{\alpha}c_{\beta})^{1/2}S_{\alpha\beta}(q)}{\left(\sum_{\alpha} b_{\alpha}c_{\alpha}\right)^2}, \quad (16)$$

$$S_x(q) = \frac{\sum_{\alpha,\beta} f_{\alpha}f_{\beta}(c_{\alpha}c_{\beta})^{1/2}S_{\alpha\beta}(q)}{\left(\sum_{\alpha} f_{\alpha}c_{\alpha}\right)^2}, \quad (17)$$

and

$$S_{zz}(q) = \frac{\sum_{\alpha,\beta} Z_{\alpha}Z_{\beta}(c_{\alpha}c_{\beta})^{1/2}S_{\alpha\beta}(q)}{\sum_{\alpha} Z_{\alpha}^2c_{\alpha}}, \quad (18)$$

where b_{α} is the coherent neutron-scattering length and f_{α} the x-ray form factor.

To the best of our knowledge, there are no diffraction experiments for liquid SiC. Calculated neutron, x-ray, and charge-charge static structure factor for the molten phases at 4000 K are shown in Fig. 15(a) and the partial structure factors are shown in Fig. 15(b). Besides the thermal effects in the height of the peaks and their broadening, the general features of $S_n(q)$ for the liquid are similar to those observed for the amorphous state.

VIII. CONCLUSIONS

We have proposed an effective interatomic interaction potential for molecular dynamics simulations of SiC. We have used the interaction potential to study structural, elastic, and dynamical properties of crystalline (3C), amorphous, and liquid states of SiC for several densities and temperatures. The potential describes correct energetics of several polymorphs (3C, 2H, and rock salt) as well as the 3C-to-rock-salt

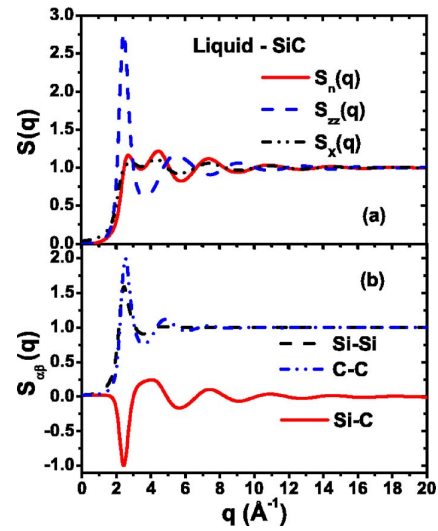


FIG. 15. (Color online) (a) Neutron, $S_n(q)$, charge-charge, $S_{zz}(q)$, and x-ray, $S_x(q)$ static structure factors calculated for molten SiC at 4000 K; (b) partial structure factors as defined in Eq. (15).

transformation pressure. For 3C-SiC, our computed elastic constants (C_{11} , C_{12} and C_{44}), melting temperature, vibrational density-of-states, and specific heat agree well with the experiments. We have predicted the elastic constants as a function of density for the crystalline and amorphous phases. We have also presented structural correlations, such as pair distribution function and neutron and x-ray static structure factors, for the amorphous and liquid states. We have successfully applied the interatomic potential to multimillion-atom molecular-dynamics simulations of sintering, indentation, fracture, and impact damage, the results of which will be presented elsewhere. Such an interatomic potential is expected to have a wide use in computational nanotechnology⁸⁹ and materials research.⁹⁰

ACKNOWLEDGMENTS

This work was partially supported by NSF, DOE, DARPA, and ARO. J.P.R. gratefully acknowledges financial support from FAPESP (Fundação de Amparo à Pesquisa do Estado de São Paulo, SP-Brazil) and CNPq (Conselho Nacional de Desenvolvimento Científico e Tecnológico–Brazil).

¹M. E. Levinshtein, S. L. Rumyantsev, and M. Shur, *Properties of Advanced Semiconductor Materials: GaN, AlN, InN, BN, SiC, SiGe* (Wiley, New York, 2001).

²D. Emin, T. L. Aselage, and C. Wood and Materials Research Society, *Novel Refractory Semiconductors: Symposium held April 21–23, 1987, Anaheim, California, USA* (Materials Research Society, Pittsburgh, 1987).

³R. C. Marshall, J. W. Faust, and C. E. Ryan, Air Force Cambridge Research Laboratories (U.S.), and University of South Carolina, *Silicon Carbide–1973; Proceedings*, 1st ed. (University of South Carolina Press, Columbia, 1974).

⁴J. R. O'Connor, J. Smiltens, and Air Force Cambridge Research Laboratories (U.S.) Electronics Research Directorate, *Silicon Carbide, a High Temperature Semiconductor; Proceedings* (Pergamon, Oxford, 1960).

⁵A. Pechenik, R. K. Kalia, and P. Vashishta, *Computer-aided Design of High-Temperature Materials* (Oxford University Press, New York, 1999).

⁶M. F. Thorpe and M. I. Mitkova and North Atlantic Treaty Organization, Scientific Affairs Division, *Amorphous Insulators and Semiconductors* (Kluwer Academic, Dordrecht, 1997).

- ⁷G. R. Fisher and P. Barnes, *Philos. Mag.* **B 61**, 217 (1990).
- ⁸R. W. G. Wyckoff, *Crystal Structures*, 2nd ed. (Interscience, New York, 1963).
- ⁹M. W. Chase, *J. Phys. Chem. Ref. Data* **14**, 633 (1985).
- ¹⁰R. M. Wentzcovitch, C. da Silva, J. R. Chelikowsky, and N. Binggeli, *Phys. Rev. Lett.* **80**, 2149 (1998).
- ¹¹S. Sampath, C. J. Benmore, K. M. Lantzky, J. Neufeind, K. Leinenweber, D. L. Price, and J. L. Yarger, *Phys. Rev. Lett.* **90**, 115502 (2003).
- ¹²D. L. Price, M. L. Saboungi, S. Susman, K. J. Volin, and A. C. Wright, *J. Phys.: Condens. Matter* **3**, 9835 (1991).
- ¹³P. Armand, M. Beno, A. J. G. Ellison, G. S. Knapp, D. L. Price, and M. L. Saboungi, *Europhys. Lett.* **29**, 549 (1995).
- ¹⁴K. Suzuya, D. L. Price, C. K. Loong, and S. W. Martin, *J. Non-Cryst. Solids* **232–234**, 650 (1998).
- ¹⁵D. D. Klug, C. A. Tulk, E. C. Svensson, and C. K. Loong, *Phys. Rev. Lett.* **83**, 2584 (1999).
- ¹⁶A. I. Kolesnikov, J. C. Li, N. C. Ahmad, C. K. Loong, J. Nipko, D. Yocum, and S. F. Parker, *Physica B (Amsterdam)* **263**, 650 (1999).
- ¹⁷A. I. Kolesnikov, J. C. Li, S. F. Parker, R. S. Eccleston, and C. K. Loong, *Phys. Rev. B* **59**, 3569 (1999).
- ¹⁸C. K. Loong, K. Suzuya, D. L. Price, B. C. Sales, and L. A. Boatner, *Physica B (Amsterdam)* **241**, 890 (1997).
- ¹⁹D. L. Price and A. J. G. Ellison, *J. Non-Cryst. Solids* **177**, 293 (1994).
- ²⁰M. Yoshida, A. Onodera, M. Ueno, K. Takemura, and O. Shimomura, *Phys. Rev. B* **48**, 10587 (1993).
- ²¹T. Sekine and T. Kobayashi, *Phys. Rev. B* **55**, 8034 (1997).
- ²²K. Strossner, M. Cardona, and W. J. Choyke, *Solid State Commun.* **63**, 113 (1987).
- ²³K. J. Chang and M. L. Cohen, *Phys. Rev. B* **35**, 8196 (1987).
- ²⁴N. E. Christensen, S. Satpathy, and Z. Pawlowska, *Phys. Rev. B* **36**, 1032 (1987).
- ²⁵K. Karch, P. Pavone, W. Windl, O. Schutt, and D. Strauch, *Phys. Rev. B* **50**, 17054 (1994).
- ²⁶K. Karch, A. Zywiets, F. Bechstedt, P. Pavone, and D. Strauch, *Silicon Carbide and Related Materials 1995* (IOP, Bristol, 1996), Vol. 142, pp. 337–340.
- ²⁷K. Karch, F. Bechstedt, P. Pavone, and D. Strauch, *J. Phys.: Condens. Matter* **8**, 2945 (1996).
- ²⁸K. Karch, P. Pavone, A. P. Mayer, F. Bechstedt, and D. Strauch, *Physica B (Amsterdam)* **220**, 448 (1996).
- ²⁹K. Karch, T. Dietrich, W. Windl, P. Pavone, A. P. Mayer, and D. Strauch, *Phys. Rev. B* **53**, 7259 (1996).
- ³⁰Y. Katayama, K. Usami, and T. Shimada, *Philos. Mag.* **B 43**, 283 (1981).
- ³¹A. Sproul, D. R. McKenzie, and D. J. H. Cockayne, *Philos. Mag.* **B 54**, 113 (1986).
- ³²P. I. Rovira and F. Alvarez, *Phys. Rev. B* **55**, 4426 (1997).
- ³³A. E. Kaloyeros, M. P. Hoffman, W. S. Williams, A. E. Greene, and J. A. Mcmillan, *Phys. Rev. B* **38**, 7333 (1988).
- ³⁴C. Meneghini, S. Pascarelli, F. Boscherini, S. Mobilio, and F. Evangelisti, *J. Non-Cryst. Solids* **137–138**, 75 (1991).
- ³⁵C. Meneghini, F. Boscherini, F. Evangelisti, and S. Mobilio, *Phys. Rev. B* **50**, 11535 (1994).
- ³⁶S. Pascarelli, F. Boscherini, S. Mobilio, and F. Evangelisti, *Mater. Sci. Eng., B* **11**, 51 (1992).
- ³⁷S. Pascarelli, F. Boscherini, S. Mobilio, and F. Evangelisti, *Phys. Rev. B* **45**, 1650 (1992).
- ³⁸J. F. Vetelino and S. S. Mitra, *Phys. Rev.* **178**, 1349 (1969).
- ³⁹C. H. Park, B. H. Cheong, K. H. Lee, and K. J. Chang, *Phys. Rev. B* **49**, 4485 (1994).
- ⁴⁰F. Finocchi, G. Galli, M. Parrinello, and C. M. Bertoni, *Phys. Rev. Lett.* **68**, 3044 (1992).
- ⁴¹V. I. Ivashchenko, P. E. A. Turchi, V. I. Shevchenko, L. A. Ivashchenko, and G. V. Rusakov, *Phys. Rev. B* **66**, 195201 (2002).
- ⁴²A. Zywiets, K. Karch, and F. Bechstedt, *Phys. Rev. B* **54**, 1791 (1996).
- ⁴³W. R. L. Lambrecht, B. Segall, M. Methfessel, and M. Vanschilfgaarde, *Phys. Rev. B* **44**, 3685 (1991).
- ⁴⁴P. C. Kelires, *Europhys. Lett.* **14**, 43 (1991).
- ⁴⁵J. Tersoff, *Phys. Rev. B* **39**, 5566 (1989).
- ⁴⁶M. J. Tang and S. Yip, *Phys. Rev. B* **52**, 15150 (1995).
- ⁴⁷L. J. Porter, J. Li, and S. Yip, *J. Nucl. Mater.* **246**, 53 (1997).
- ⁴⁸J. Li, L. Porter, and S. Yip, *J. Nucl. Mater.* **255**, 139 (1998).
- ⁴⁹A. Noreyan, J. G. Amar, and I. Marinescu, *Mater. Sci. Eng., B* **117**, 235 (2005).
- ⁵⁰M. Tang and S. Yip, *J. Appl. Phys.* **76**, 2719 (1994).
- ⁵¹A. Catellani, G. Galli, and F. Gygi, *Phys. Rev. Lett.* **77**, 5090 (1996).
- ⁵²X. Luo, G. F. Qian, W. D. Fei, E. G. Wang, and C. F. Chen, *Phys. Rev. B* **57**, 9234 (1998).
- ⁵³S. Y. Karpov, Y. N. Makarov, and M. S. Ramm, *Phys. Status Solidi B* **202**, 201 (1997).
- ⁵⁴R. Devanathan, W. J. Weber, and F. Gao, *J. Appl. Phys.* **90**, 2303 (2001).
- ⁵⁵F. Gao, E. J. Bylaska, W. J. Weber, and L. R. Corrales, *Nucl. Instrum. Methods Phys. Res. B* **180**, 286 (2001).
- ⁵⁶L. Malerba, J. M. Perlado, A. Sanchez-Rubio, I. Pastor, L. Colombo, and T. D. de la Rubia, *J. Nucl. Mater.* **283–287**, 794 (2000).
- ⁵⁷L. Malerba and J. M. Perlado, *J. Nucl. Mater.* **289**, 57 (2001).
- ⁵⁸H. C. Huang, N. M. Ghoniem, J. K. Wong, and M. I. Baskes, *Model. Simul. Mater. Sci. Eng.* **3**, 615 (1995).
- ⁵⁹E. Pearson, T. Takai, T. Halicioglu, and W. A. Tiller, *J. Cryst. Growth* **70**, 33 (1984).
- ⁶⁰P. Erhart and K. Albe, *Phys. Rev. B* **71**, 035211 (2005).
- ⁶¹D. Brenner, *Phys. Status Solidi B* **217**, 23 (2000).
- ⁶²F. Gao and W. J. Weber, *Nucl. Instrum. Methods Phys. Res. B* **191**, 504 (2002).
- ⁶³F. Shimojo, I. Ebbsjo, R. K. Kalia, A. Nakano, J. P. Rino, and P. Vashishta, *Phys. Rev. Lett.* **84**, 3338 (2000).
- ⁶⁴M. Catti, *Phys. Rev. Lett.* **87**, 035504 (2001).
- ⁶⁵M. S. Miao and W. R. L. Lambrecht, *Phys. Rev. Lett.* **94**, 225501 (2005).
- ⁶⁶H. Kikuchi, R. K. Kalia, A. Nakano, P. Vashishta, P. S. Branicio, and F. Shimojo, *J. Appl. Phys.* **98**, 103524 (2005).
- ⁶⁷A. Rahman and P. Vashishta, in *The Physics of Superionic Conductors and Electrode Materials*, edited by W. Perran (Plenum, New York, 1983), p. 83.
- ⁶⁸P. Vashishta and A. Rahman, *Phys. Rev. Lett.* **40**, 1337 (1978).
- ⁶⁹P. Vashishta, J. N. Mundy, and G. K. Shenoy, in *Proceedings of the International Conference on Fast Ion Transport in Solids, Electrodes, and Electrolytes, Lake Geneva, Wisconsin, May 21–25, 1979* (North Holland, New York, 1979).
- ⁷⁰F. H. Stillinger and T. A. Weber, *Phys. Rev. B* **31**, 5262 (1985).
- ⁷¹P. N. Keating, *Phys. Rev.* **145**, 637 (1966).
- ⁷²P. S. Branicio, J. P. Rino, F. Shimojo, R. K. Kalia, A. Nakano, and P. Vashishta, *J. Appl. Phys.* **94**, 3840 (2003).
- ⁷³P. Vashishta, R. K. Kalia, G. A. Antonio, and I. Ebbsjo, *Phys. Rev. Lett.* **62**, 1651 (1989).
- ⁷⁴P. Vashishta, R. K. Kalia, J. P. Rino, and I. Ebbsjo, *Phys. Rev. B* **41**, 12197 (1990).
- ⁷⁵M. P. Allen and D. J. Tildesley, *Computer Simulation of Liquids* (Clarendon, Oxford, 1987).
- ⁷⁶A. Nakano, R. K. Kalia, and P. Vashishta, *J. Non-Cryst. Solids* **171**, 157 (1994).
- ⁷⁷F. D. Murnaghan, *Proc. Natl. Acad. Sci. U.S.A.* **30**, 244 (1944).
- ⁷⁸R. I. Scace and G. A. Slack, in *Silicon Carbide—A High Temperature Semiconductor*, edited by J. R. O'Connor and J. Smiltens (Pergamon, Oxford, 1960), p. 24.
- ⁷⁹J. F. Nye, *Physical Properties of Crystals: Their Representation by Tensors and Matrices* (Clarendon/Oxford University Press, Oxford, 1984).
- ⁸⁰P. Hohenber and W. Kohm, *Phys. Rev.* **136**, B864 (1964).
- ⁸¹W. Kohn and P. Vashishta, in *Theory of the Inhomogeneous Electron Gas*, edited by S. L. Lundqvist and N. H. March (Plenum Press, New York, 1983), p. 79.
- ⁸²F. Shimojo, R. K. Kalia, A. Nakano, and P. Vashishta, *Comput. Phys. Commun.* **140**, 303 (2001).
- ⁸³M. L. Cohen, *Science* **261**, 307 (1993).
- ⁸⁴G. Kresse and J. Hafner, *Phys. Rev. B* **49**, 14251 (1994).
- ⁸⁵E. B. Tadmor and S. Hai, *J. Mech. Phys. Solids* **51**, 765 (2003).
- ⁸⁶H. Bilz and W. Kress, *Phonon Dispersion Relations in Insulators* (Springer, Berlin, 1979).
- ⁸⁷L. V. Gurvich, I. V. Veyts, and C. B. Alcock, *Thermodynamic Properties of Individual Substances*, 4th ed. (Hemisphere, New York, 1989).
- ⁸⁸J. P. Rino, I. Ebbsjo, P. S. Branicio, R. K. Kalia, A. Nakano, F. Shimojo, and P. Vashishta, *Phys. Rev. B* **70**, 045207 (2004).
- ⁸⁹D. Srivastava and S. N. Atluri, *Comput. Model. Eng. Sci.* **3**, 531 (2002).
- ⁹⁰B. B. Karki, R. M. Wentzcovitch, S. de Gironcoli, and S. Baroni, *Science* **286**, 1705 (1999).
- ⁹¹W. A. Harrison, *Electronic Structure and the Properties of Solids: The Physics of the Chemical Bond* (Freeman, San Francisco, 1980).
- ⁹²<http://www.ioffe.ru/SVA/NSM/> (Ioffe Institute, 2003).
- ⁹³R. D. Carnahan, *J. Am. Ceram. Soc.* **51**, 223 (1968).
- ⁹⁴D. W. Feldman, J. H. Parker, W. J. Choyke, and L. Patrick, *Phys. Rev.*

173, 787 (1968).

⁹⁵I. V. Aleksandrov, A. F. Goncharov, S. M. Stishov, and E. V. Yakovenko, JETP Lett. **50**, 127 (1989).

⁹⁶G. L. Harris *et al.*, in *Properties of Silicon Carbide*, edited by G. L. Harris,

EMIS Data Reviews Series, N13 (INSPEC, London, 1995), p. 8.

⁹⁷*Physics of Group IV-V Elements and III-V Compounds*, edited by O. Madelung *et al.*, Landolt-Bornstein, New Series, Group II, Vol. 17a (Springer, Berlin, 1982), p.136.